Semicond. Sci. Technol. **33** (2018) 095024 (7pp) https://doi.org/10.1088/1361-6641/aad539

Fast estimation of channel temperature in GaN high electron mobility transistor under RF operating conditions

Boris Chervonni[1], **Oleg Aktushev**[2], **Efi Ojalvo**[2], **Yaron Knafo**[2], **Yury Turkulets**[1] and **Ilan Shalish**[1]

[1] Department of Electrical and Computer Engineering, Ben Gurion University of the Negev, Beer Sheva, 8410501, Israel
[2] Gal-El (MMIC), Ashdod 77102, Israel

E-mail: shalish@ bgu.ac.il

Received 23 April 2018, revised 10 July 2018
Accepted for publication 23 July 2018
Published 28 August 2018

Abstract

Working at high RF power leads gallium nitride (GaN) high electron mobility transistors (HEMT) to self-heating that poses a limit to device performances and reliability. Thermal characterization is therefore of great value for proper design of heat dissipation and also for device reliability studies. The peak power dissipation in HEMT devices is located in the channel near the gate edge, which is typically buried under a field plate. This hot spot is thus inaccessible to direct temperature measurement. Therefore, any method used for temperature measurement has to be augmented by a thermal simulation to calculate the actual temperature in the channel from temperature measured elsewhere. In this work, we used thermal imaging to measure temperature during device operation in various pulsed RF conditions. To obtain the hot spot temperature, we developed a thermal simulation of AlGaN/GaN HEMT transistor on SiC substrate. The simulation estimates the channel temperature using 3D finite element method with multi-parameter input. To calibrate the simulation, we compared simulation results with IR images of a 2 mm AlGaN/GaN HEMT transistor operating at various pulsed RF conditions. The simulation is typically slow. In this work, we used the calibrated simulation to study the hot spot temperature as a function of the working conditions and formulated an approximated equation for the thermal behavior of the transistor as a function of power dissipation, base plate temperature, pulse width, and pulse duty cycle that may be used to estimate the channel temperature in real time.

Keywords: HEMT, GaN, RF, thermal model, IR imaging

(Some figures may appear in colour only in the online journal)

1. Introduction

GaN HEMT transistors grown on SiC substrates are receiving much attention due to their high performance in producing high RF power at microwave frequencies. This makes them a promising technological solution for many civil and military applications [1–3]. Features such as high sheet charge density at the two-dimensional electron gas hetero-interface [4], high saturation velocity, high electron mobility, and high critical field for breakdown [5], enable GaN HEMT devices to reach high currents and high operating voltages, leading to their remarkable capability of handling high RF power. Unfortunately, the high power density in the AlGaN/GaN HEMT leads to self-heating which may be detrimental to transistor performance and reliability [6, 7]. An important figure of merit for reliability of HEMT is the device mean-time-to-failure (MTTF). MTTF is typically predicted by correlating channel temperature with a thermal Arrhenius model [8]. Hence, to calculate the correct MTTF, one is required to know the channel temperature. However, a direct measurement of the hot spot above the channel near the gate edge where the electric field reaches its maximum [9–12], is not possible, because this point is concealed by the field plate [5]. Therefore, the only way to obtain this temperature is to estimate it using thermal simulations. This estimation requires a thermal model calibrated using a temperature measured elsewhere. Several works on measuring temperature in AlGaN/GaN HEMT devices in DC or DC pulse mode [9, 10, 13, 14], and RF mode [15], have been reported. This study was inspired by the work of Baczkowski *et al* [15]. In their model, the temperature is derived from the dissipated power alone. However, we were interested in pulsed RF conditions where the pulse characteristic parameters have a critical role in defining the temperature. Hence, we had to add in this study the influence of pulse width and pulse duty cycle producing a *multiple input simulation*. Our temperature characterization was carried out using an infrared microscope over a range of RF conditions at pulse mode and the results were compared with the results of a finite element analysis (FEA) using the Comsol software. The measurements were used to calibrate the thermal simulation model of AlGaN/GaN HEMT over a wide range of RF conditions, and the calibrated thermal simulation was then used to study the dynamics of the hot spot temperature and develop a model for the thermal behavior of the hot spot.

We note that there exist alternative ways to assess the temperature other than IR imaging. These include, for example, microRaman, gate resistance, and thermoreflectance [16]. In order to work at true RF conditions and measure several devices to gain statistics, we had to work on the complete wafer and operate the devices using probes. Under pulse RF conditions, the planar position of the probes is critical to maintain the correct phase. Hence, it was not possible to flip the wafer over and access its back side, e.g., to carry out back side Raman measurements. To carry out the gate resistance method would require working in short enough pulses to avoid self-heating, but this would not allow measuring under the real operating conditions of the device. On the other hand, IR imaging could certainly be replaced by thermoreflectance, which is by far the most accurate and high resolution method for measuring electronic device temperature today and this would certainly improve the accuracy and reduce the uncertainties of the measurement. However in principle, the method we present would not change. It will only have a more accurate calibration.

2. Experimental details

2.1. Device structure

The AlGaN/GaN structure was grown on a SiC substrate by metal-organic chemical vapor deposition (MOCVD). The device fabrication included isolation by ion implantation, Ti/Al Ohmic contacts, SiN passivation, T-gate formation, and thick transmission lines using air bridge technology. This was followed by a back side process to thin down the substrate to 100 μm, and plating of the back side with Au. The device studied in this paper had 10 gate-fingers and the width of each finger was 200 μm and length 0.25 μm. The drain-source distance was 5 μm. Each gate was totally covered by a field plate. The wafer placed onto a temperature controlled 8 inch chuck with a temperature accuracy of ± 1 °C. Temperature measurements and load-pull measurements were carried out directly on the (non-diced) wafer so no assembly was actually required. On the other hand, since the measurements are carried out using probes, it is not possible to flip the wafer over and measure from its back side, i.e., this setup does not allow front to back measurements, as those required, for example, in the Raman method in order to probe under the field plate (e.g., as in [17]).

2.2. Electrical characterization

Electrical characterization was carried out using a load-pull system (vector network analyzer based load-pull system from Amcad Engineering) [18, 19]. The frequency for the load-pull measurement was 3.5 GHz. The RF power sweep was carried out in deep class AB ($I_{DS} = 200$ mA $V_{DS} = 30$ V), and all devices were matched for maximum output power impedance. During the infrared microscope imaging, the devices were operated in pulse mode. Imaging was carried out in these 4 specific combinations of pulse width and duty cycle: 10 μs/10%, 100 μs/10%, 100 μs/20% and 300 μs/20%. Before infrared imaging, the devices were characterized in RF pulse mode (at a pulse width of 100 μs and duty cycle 10%), the frequency was 3.5 GHz at maximum output power impedance, and the device was biased at $V_{DS} = 30$ V $I_{DS} = 200$ mA. All measurements (current and power) were carried out while the pulse was on (150 measurements per pulse). As the purpose of this method was to evaluate the transistor thermal parameters in the *typical* working conditions of the specific device, where the pulses are typically long, self-heating cannot be avoided, and therefore, gate resistance measurement were not an option.

2.3. Infrared thermography

Infrared thermography measures temperature by measuring the intensity of infrared radiation which is relative to the object temperature. To this end, we used an infrared microscope (Quantum Focus Instruments Corp.). Using this instrument, one can acquire 2D thermal maps of microelectronics devices [20–22]. Infrared thermography is based on Planck's law of black body radiation [23]. However, Planck's law was derived for a black body, a perfect absorber material that does not reflect or transmit any light. For materials that are not a perfect black body, a correction has to be made, which is called the emissivity, ε. Emissivity, ε, is the ratio of the actual material radiance to that of a perfect black body as predicted by Planck's law for the same temperature and wavelength.

Our thermal images were acquired at the wavelength range of 3–5 μm. In all measurements a 12$\times$ infrared (IR) objective (N.A $= 0.85$) was used and a single element InSb detector which dimensions were 250 μm $\times$ 250 μm and its spatial resolution was 20.8 μm. The temperature was

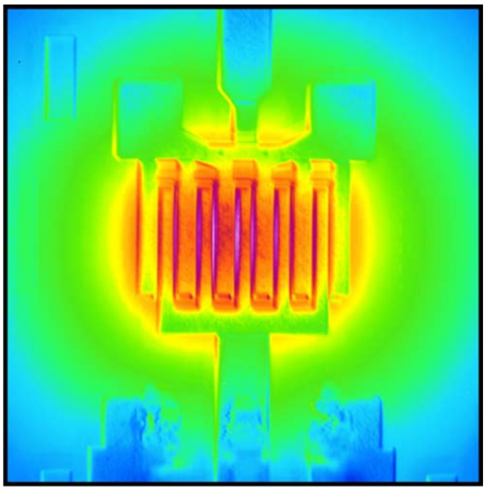

Figure 1. Thermal image of a typical HEMT device taken using the InSb 512 × 512 detector. Total imaged area is 3.7 mm by 3.7 mm. The thermal measurements in this work were not carried out by this image sensor, but rather by a single element detector.

measured during load-pull measurements in the various conditions using a load-pull setup under the IR microscope.

The wafer was placed onto a thermal chuck and infrared imaging of the surface was carried out. To calibrate the infrared microscope, one has to measure the intensity of infrared radiation of the investigated part of a non-biased device heated to a known temperature (in our case 150 °C and 170 °C) measured using a thermocouple.

From this measurement, emissivity can be calculated for each pixel. The resulting emissivity map is then used to compute the temperature from the raw-infrared intensity-data of the powered device [21]. Another emissivity that had to be taken into account is the changing emissivity of the electronic circuit of the infrared microscope itself [21]. Following this calibration, thermal scans at different dissipated power levels of AlGaN/GaN HEMT were acquired. Figure 1 shows a typical thermal map of a device operated in CW. Note that in this work, we have characterized the device under pulse RF operating conditions and not CW. This figure is given only to illustrate the thermal emission from the device.

For thermography in RF pulse mode, the devices were biased at 30 V and $I_{DS} = 200$ mA at the various RF pulse conditions. All RF measurements were carried out at a frequency of 3.5 GHz at maximum output power impedance, and dissipated power sweep was performed from 5 to 8 W. The base plate temperatures at the infrared microscope chuck during these temperature measurements was maintained at 150 °C or 170 °C.

Temperature measurements in pulse mode were carried out while the pulse was on, and they were later compared with simulated temperature that was also sampled when the pulse was on.

2.4. Thermal simulation

A 3D thermal model was constructed to simulate the temperature as a function of position within the volume of the transistor. There are several alternative methods to perform a thermal simulation. In this work, we used the finite element method (FEM). In this method, the volume of the simulated part is viewed as subdivided into a finite number of elements, each having its own thermal properties. In our simulation, we used 731 803 tetrahedron-shaped elements. For each such element, each of the following thermal equations has to be solved separately:

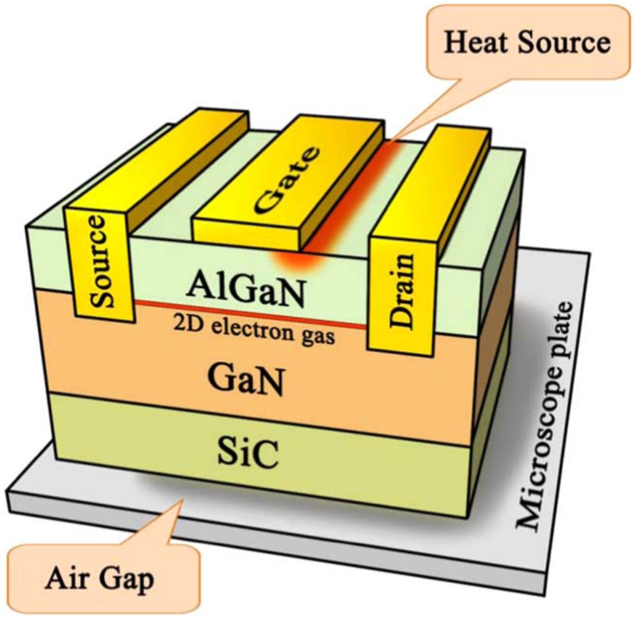

Figure 2. Schematic structure of the device layers and the air-gap between the device and the microscope stage used for the thermal simulation. For clarity, the device is drawn without the field plate.

$$\rho C_p \frac{\partial T}{\partial t} = \nabla(k \nabla T) + Q, \tag{1}$$

$$\overrightarrow{Q} = -k \overrightarrow{\nabla} T, \tag{2}$$

where ρ is the mass density, C_P is the heat capacity at a constant pressure, k is the thermal conductivity, T is the temperature, and Q is the heat flux. Our thermal model was created using Comsol—a commercial FEM software [24]. Most of the thermal properties, including temperature dependent properties (thermal conductivity, density, and heat capacity at constant pressure) of the various materials used in the simulation were those available in the Comsol database. Heat capacity and thermal conductivity of SiC were taken from Nilsson *et al* [25]. The device structure and the targeted area for infrared thermography are shown in figure 2. An important part that was added to the simulated structure is the air-gap between the device and the microscope plate. The microscope plate was grooved with very shallow grooves that contain air. We simulated them using a uniform layer of air. The thickness of that air-gap was used to calibrate the simulation result to fit the measured temperature. Figure 3 shows a drawing of the on-projection of the simulated device and the position of the imaged and simulated pixel. The heat source was defined all over the cross-section area of the channel using the following equation:

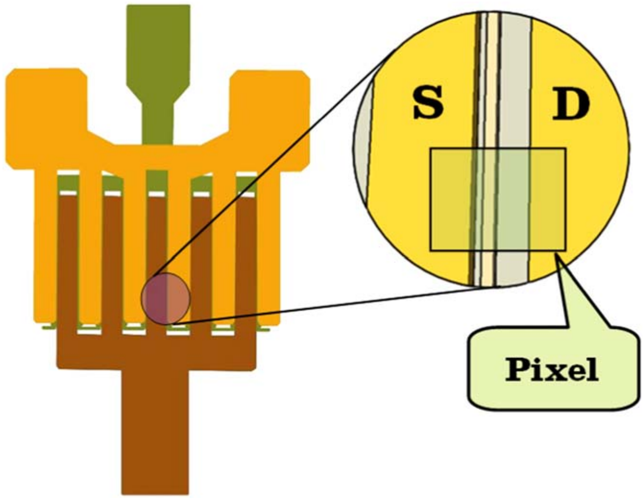

Figure 3. On-projection of the simulated device showing the device finger structure, the green rectangle is the area of the surface pixel for which the temperature is calculated. The calculated temperature is then compared to temperature obtained from the IR image pixel of the same position and area. For clarity, the device is drawn without the field plate.

$$Q = \frac{P_D}{w \cdot l \cdot h} \cdot \#G \cdot \mathrm{an1}(t), \quad (3)$$

where $\#G$ is the number of gates in the device, w and h, are the channel cross-section dimensions, and l is the length of the heat source, starting at the drain-side of the gate and extending to a distance l towards the source. The dimension l was a region within which the electric field exceeded a threshold value and was obtained from ATLAS/Blaze (SILVACO) simulation of the electric field [9–12]. An1(t) is a pulse function which equals 1 when the pulse is on**.** The thermal resistance of the interface between GaN and the SiC substrate has been reported to be negligible [26].

2.5. Thermal model for surface pixel

To evaluate the performance of the simulation, we compared the calculated and the measured temperatures on the same surface spot under different operating conditions of the device and adjusted the air-gap to obtain the closest match between simulated and measured temperature. To evaluate the result, we present each of these temperatures (the calculated and the measured) as a function of the operating parameters. This data was eventually fitted using the commercial statistical software JMP [27] to obtain empirical functions that calculate the temperatures from the given operating conditions of the device.

Two functions were generated to describe the simulated and the measured temperatures as functions of the four operating parameters:

$$T_{\mathrm{Sim}} = a_S + b_S \cdot T_{\mathrm{BP}} + c_S \cdot P_D + d_S \cdot \mathrm{PW} + e_S \cdot D, \quad (4)$$

$$T_{\mathrm{Meas}} = a_M + b_M \cdot T_{\mathrm{BP}} + c_M \cdot P_D + d_M \cdot \mathrm{PW} + e_M \cdot D, \quad (5)$$

where T_{Sim} is the simulated temperature as a function of the pulse width, PW, pulse duty cycle, D, dissipated power in Watts, P_D, and temperature of the base plate of the microscope chuck in Celsius, T_{BP}. T_{Meas} is the measured temperature. The coefficients are

$$a_S = -45.55 \pm 21.16\ ^{\circ}\mathrm{C}, \quad b_S = 1.14 \pm 0.12,$$
$$c_S = 5.79 \pm 1.12\ ^{\circ}\mathrm{C\ W^{-1}}, \quad d_S = 0.11 \pm 0.018\ ^{\circ}\mathrm{C}\ \mu\mathrm{s}^{-1},$$
$$e_S = 0.43 \pm 0.36\ ^{\circ}\mathrm{C}, \quad a_M = -50.87 \pm 6.44\ ^{\circ}\mathrm{C},$$
$$b_M = 1.16 \pm 0.04, \quad c_M = 6.04 \pm 0.42\ ^{\circ}\mathrm{C\ W^{-1}},$$
$$d_M = 0.08 \pm 0.004\ ^{\circ}\mathrm{C}\ \mu\mathrm{s}^{-1}, e_M = 0.14 \pm 0.10\ ^{\circ}\mathrm{C}.$$

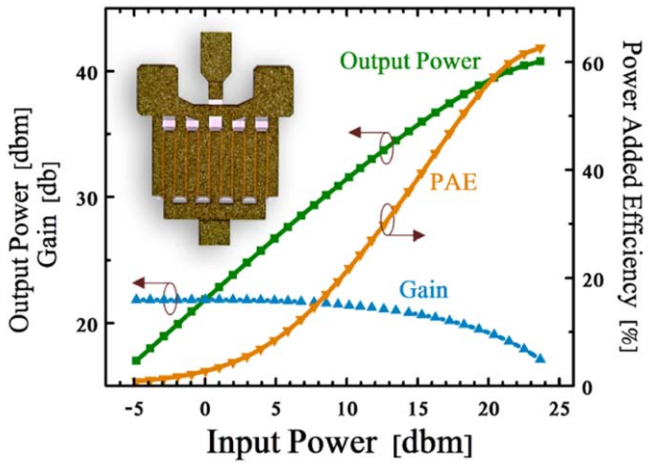

Figure 4. Performance characteristics of the device chosen for this study. Output power, gain, and power added efficiency (PAE) are shown as a function of the input power. The inset shows an optical image of the device. Room temperature measurements were carried out at pulse mode (pulse width 100 μs and pulse duty cycle 10%) at 3.5 GHz. The device was biased at $V_{\mathrm{DS}} = 30$ V and $I_{\mathrm{DS}} = 200$ mA.

3. Results and discussion

3.1. Device performance

Figure 4 shows the performance characteristics of the device chosen for this study. Output power, gain, and power added efficiency (PAE) are shown as a function of the input power. The inset shows an optical image of the device.

3.2. Thermal model performance for surface pixel

Figure 5 compares the temperature of the measured surface pixel, averaged over a set of 5 transistors (dots), with the simulated temperature (full line) calculated for the same pixel location and for the same conditions. The left panel is for a base plate temperature of 150 °C, while the right panel is for a base plate temperature of 170 °C. The temperatures are presented as a function of the dissipated power. The different colors represent the 4 operating conditions tested in the pulse mode:

(a) PW = 10 μs, D = 10%,
(b) PW = 100 μs, D = 10%,
(c) PW = 100 μs, D = 20%,
(d) PW = 300 μs, D = 20%.

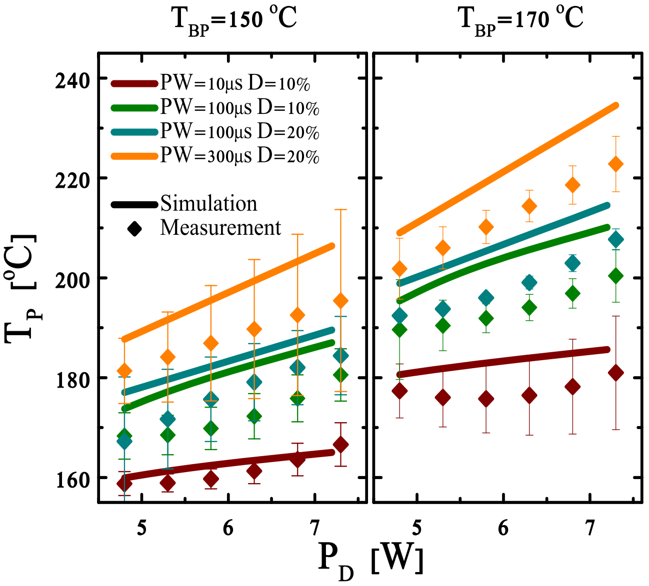

Figure 5. Comparison of simulated temperature (lines) and measured temperature (dots) of the surface pixel (at the position showed in figure 3) as a function of the dissipated power measured at two base plate temperatures: 150 °C (left Column) and 170 °C (right column) under 4 different operating conditions represented by the different colors.

The figures show the goodness of the simulation and how close it can predict the measured temperatures.

So far, we have presented a method by which we measure the surface pixel temperature and a method by which we simulate the same temperature. We then used the measured temperature to calibrate the simulation. Once the simulation is calibrated properly, we can use it to predict the temperature at the channel by entering the channel coordinates instead of the surface pixel coordinates. However, we first need to evaluate the goodness of our model functions for the surface pixel. To this end, we will now compare the results of the model functions with measured temperatures. Figure 6 compares measured and model-calculated temperatures at various pulse mode conditions. The best correlation is when $y = x$. As can be seen, most of the data points fall close to that line. The correlation calculated for this plot was $R^2 = 0.94$. The actual T_{Sim} function has five-dimensions and therefore cannot be drawn on a 2D graph. Figure 7 shows a correlation of $R^2 = 0.90$ between data from direct temperature measurement of the surface pixel and the function that fits these data, T_{Meas}, which testifies for a fairly good fit.

3.3. Channel temperature model

Once our simulation was calibrated using the IR microscopy imaging for the pulse mode, we could use the simulation to explore the dependence of the channel temperature, which cannot be measured, on the various operation parameters of the transistor.

Figure 8 shows the (simulated) channel temperature as a function of the dissipated power, P_D, for base plate temperatures of 150 °C and 170 °C. Since the simulation uses intensive calculations, it is slow and is not practical for use in

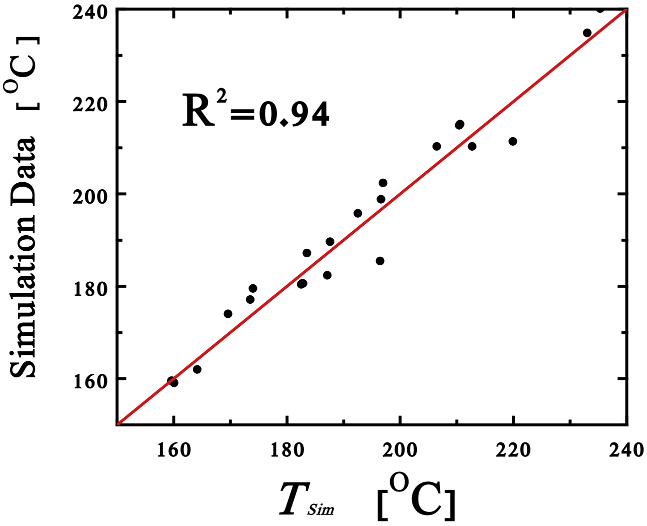

Figure 6. Simulation data shown as a function of the fitting function that fits it. The red line shows were the perfect correlation of $R^2 = 1.0$ would be. The correlation coefficient is found to be $R^2 = 0.94$. The actual function has five-dimensions and cannot be drawn on a 2D graph.

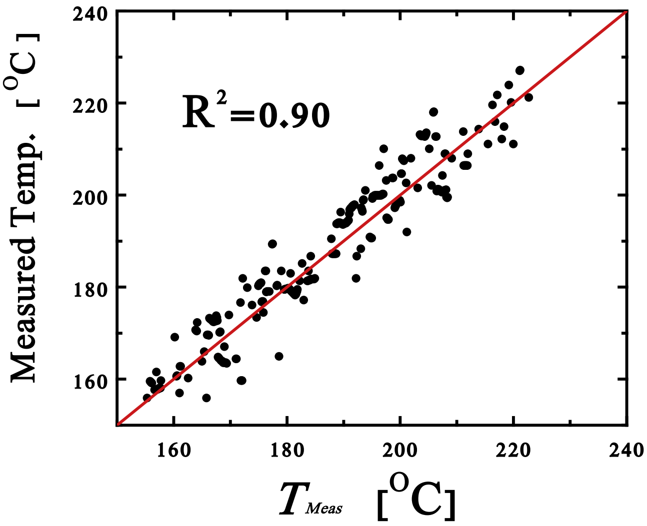

Figure 7. Measured temperature of the surface pixel in pulse mode shown as a function of the fitting function that fits it. The red line shows were the perfect correlation of $R^2 = 1.0$ would be. The correlation coefficient is found to be $R^2 = 0.90$. The actual function has five-dimensions and cannot be drawn on a 2D graph.

real time application such as a reliability machine as part of reliability tests. To produce a faster means to obtain a simulated value of the channel temperature, we used the commercial statistical software JMP [24] to fit the data calculated using the simulation in order to obtain an expression that can produce the results in real time. Within the limits of the parameter space chosen for this study, we found that the channel temperature of the device studied can be predicted reliably by the fairly simple expression:

$$T_{\mathrm{Channel}} = a_C + b_C \cdot T_{\mathrm{BP}} + c_C \cdot P_D + d_C \cdot \mathrm{PW} + e_C \cdot D, \quad (6)$$

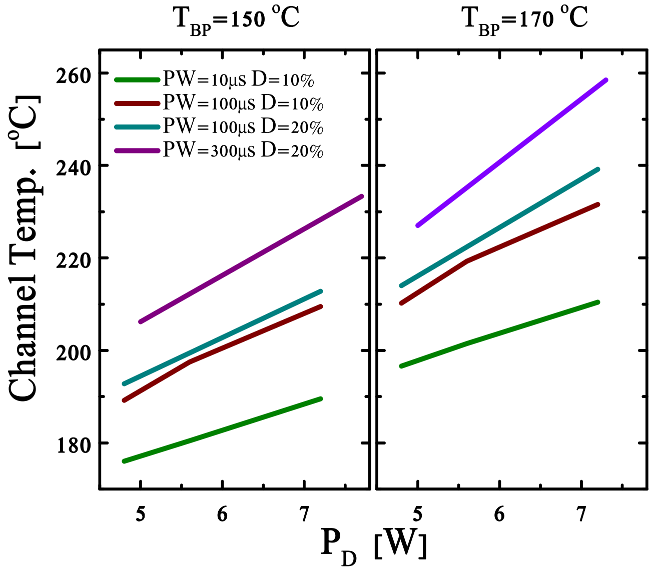

Figure 8. Simulated channel temperature as a function of the dissipated power, P_D, for base plate temperatures of 150 °C and 170 °C. Note the difference from figure 5 which relate to the same area on the surface, while this figure shows simulation data deep under the gate. Also note that the simulation element is $0.2 \times 0.2\ \mu m^2$.

where the coefficients are

$$a_C = -47.26 \pm 20.25\ ^\circ\mathrm{C}, \quad b_C = 1.15 \pm 0.12,$$
$$c_C = 9.06 \pm 1.07\ ^\circ\mathrm{C\ W^{-1}}, \quad d_C = 0.11 \pm 0.02\ ^\circ\mathrm{C}\ \mu\mathrm{s}^{-1},$$
$$e_C = 0.50 \pm 0.35\ ^\circ\mathrm{C}.$$

This fit is valid for the following parameter ranges:

$$150\ ^\circ\mathrm{C} \leqslant T_{\mathrm{BP}} \leqslant 170\ ^\circ\mathrm{C},\ 4\ \mathrm{W} \leqslant P_D \leqslant 8\ \mathrm{W},$$
$$10\ \mu\mathrm{S} \leqslant \mathrm{PW} \leqslant 300\ \mu\mathrm{S},\ 10\% \leqslant D \leqslant 20\%.$$

The goodness of the fit is shown in figure 9 that shows the results of the thermal model as a function of their fit, as given in equation (6). The correlation coefficient calculated for figure 9 is $R^2 = 0.96$. This means that, under pulse mode conditions, equation (6) provides a reliable description of the channel temperature.

Equation (6) is a *linear approximation* of the relations between the four input parameters and the channel temperature. Other methods to obtain the same, such as lumped circuit models of thermal impedances, are unlikely to provide better accuracy within the limits of the parameter range studied here, because within the studied range and the observed uncertainties, the observed behavior is very close to linear [28]. Furthermore, thermal impedances have been used to describe the relation between temperature and the dissipated power. However, our model takes into account several more input parameters, such as the pulse width and duty cycle which do not simply relate to the temperature via thermal impedances.

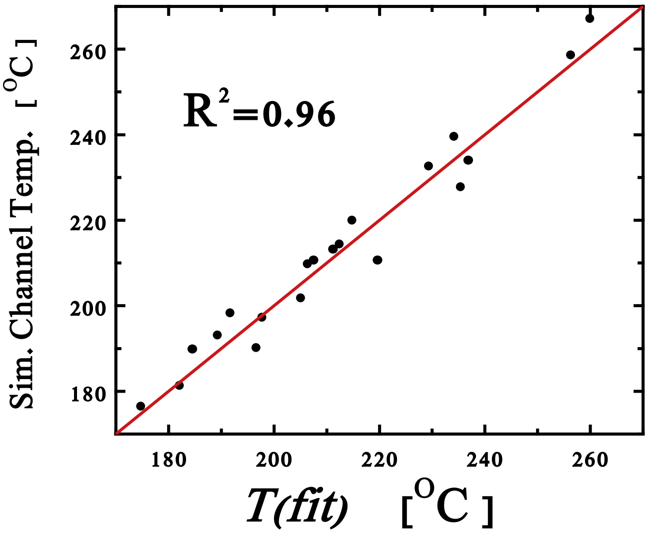

Figure 9. Simulated channel temperature at various conditions in pulse mode shown as a function of the temperature calculated by its fitting function (equation (6)). The red line shows were the perfect correlation of $R^2 = 1.0$ would be. The correlation coefficient is found to be $R^2 = 0.96$. The actual function has five-dimensions and cannot be drawn on a 2D graph.

4. Conclusion

In this work, we developed and calibrated a thermal simulation for a specific GaN HEMT device, which takes into account parameters, such as base plate temperature, pulse width and pulse duty cycle, in addition to the dissipated power, to simulate the highest temperature developed in the device. Adding these parameters provides a more complete and accurate simulation than ever before. We used the simulation to study the thermal behavior of the device within the relevant parameter space and to obtain an equation that describes the hot spot temperature as a function of all these studied parameters. The resulting equation provides an important experimental handle in the study of the optimal working point, for identifying the thermal limits in the parameter space, and to provide a better understanding of the device performance at various working conditions. The resulting equation also provides a tool for the designer of a heat-sink for a transmitter/receiver RF module. It also provides a means for a fast estimate that is more suitable to the requirements of reliability machines and thus allows to characterize the reliability and lifetime of the device.

Acknowledgements

The authors would like to thank the Gal-El (mmic) R&D group and Gal-El (mmic) management headed by Dr Edna Manheim, for their support and for making this research possible. The work at Ben Gurion University was funded by the Israeli Ministry of Defense (MAFAT).

ORCID iDs

Yury Turkulets https://orcid.org/0000-0002-8383-0231
Ilan Shalish https://orcid.org/0000-0002-8053-7339

References

[1] Mishra U K, Shen L, Kazior T E and Wu Y-F 2008 GaN-based RF power devices and amplifiers *Proc. IEEE* **96** 287
[2] Uren M J, Barnes A R, Martin T, Balmer R S, Hilton K P, Hayes D G and Kuball M 2002 GaN devices for microwave applications [FET/HEMT] *Proc. 10th IEEE Int. Symp. Electron Devices Microw. Optoelectron. Appl. (EDMO) (Manchester, UK)* pp 111–8
[3] Trew R J, Bilbro G L, Kuang W, Liu Y and Yin H 2005 Microwave AlGaN/GaN HFETs *IEEE Microw. Mag.* **6** 56
[4] Ambacher O *et al* 2000 *J. Appl. Phys.* **87** 334
[5] Karmalkar S and Mishra U K 2001 Enhancement of breakdown voltage in AlGaN high electron mobility transistors using a field plate *IEEE Trans. Electron Devices* **48** 1515
[6] McAlister S P, Bardwell J A, Haffouz S and Tang H 2006 Self-heating and the temperature dependence of the dc characteristics of GaN heterostructure field effect transistors *J. Vac. Sci. Technol.* A **24** 624
[7] Meneghesso G, Verzellesi G, Danesin F, Rampazzo F, Zanon F, Tazzoli A, Meneghini M and Zanoni E 2008 Reliability of GaN high-electron-mobility transistors: state of the art and perspectives *IEEE Trans. Device Mater. Reliab.* **8** 332
[8] Grundbacher R, Callejo L, Kan Q, Lai R, Liu P H, Eng D and Oki A 2004 Degradation of AlGaN/GaN HEMTs under elevated temperature lifetesting *Microelectron. Reliab.* **44** 1033
[9] Aubry R, Jacquet J-C, Weaver J, Durand O, Dobson P, Mills G, di Forte-Poisson M-A, Cassette S and Delage S-L 2007 STHM temperature mapping and nonlinear thermal resistance evolution with bias on AlGaN/GaN HEMT devices *IEEE Trans. Electron Devices* **54** 385
[10] Jacquet J-C, Aubry R, Gérard H, Delos E, Rolland N, Cordier Y, Bussutil A, Rousseau M and Delage S-L 2004 Analytical transport model of AlGaN/GaN HEMT based on electrical and thermal measurement *Proc. 12th GAAS Symp. (Amsterdam, The Netherlands)* pp 235–8
[11] Onodera H and Horio K 2012 Physics-based simulation of field-plate effects on breakdown characteristics in AlGaN/GaN HEMTs *Proc. 7th IEEE/EuMIC (Amsterdam, The Netherlands)* pp 401–4
[12] Hosch M, Behtash R, Thorpe J R, Held S, Blanck H, Riepe K and Schumacher H 2008 The impact of layout and technology on the DC and RF performance of AlGaN/GaN HFETs *Proc. Asia-Pacific Microwave Conf., (APMC) (Macau, China)* pp 1–4
[13] Pichonat E, Kuzmik J, Bychikhin S, Pogany D, Poisson M A, Grimbert B and Gaquiere C 2006 Temperature analysis of AlGaN/GaN high-electronmobility transistors using micro-Raman scattering spectroscopy and transient interferometric mapping *Proc. Microwave Integrated Circuits Conf. (EuMIC) (Manchester, UK)* pp 54–7
[14] Simms R J T, Pomeroy J W, Uren M J, Martin T and Kuball M 2008 Channel temperature determination in high-power AlGaN/GaN HFETs using electrical methods and Raman spectroscopy *IEEE Trans. Electron Devices* **55** 478
[15] Baczkowski L, Jacquet J C, Jardel O, Gaquiere C, Moreau M, Carisetti D, Brunet L, Vouzelaud F and Mancuso Y 2015 Thermal characterization using optical methdos of AlGaN/GaN HEMTs on SiC substrate in RF operating conditions *IEEE Trans. Electron Dev.* **62** 3392
[16] Cahil D G, Goodson K and Majumdar A 2002 Thermometry and thermal transport in micro/nanoscale solid-state devices and structures *J. Heat Transfer* **124** 223
[17] Martin-Horcajo S, Pomeroy J W, Lambert B, Jung H, Blanck H and Kuball M 2015 Transient thermoreflectance for gate temperature assessment in pulse operated GaN based HEMTS *IEEE Electron Dev Letters.* **37** 1197
[18] Gao S and Park C W 2012 Large signal characterization of GaN HEMT transistor by multi-harmonic source & load-pull tuner system *80th ARFTG Microwave Measurement Conf. (San Diego, CA)*
[19] Dudkiewicz S, Tenberge M S, Esposito G and Barbieri T 2015 Understanding the relevance of harmonic impedance matching in amplifier design *Microw. Mag.* **58** 112
[20] Das J, Oprins H, Ji H, Sarua A, Ruythooren W, Derluyn J, Kuball M, Germain M and Borghs G 2006 Improved thermal performance of AlGan/GaN HEMTs by an optimized flip-chip design *IEEE Trans. Electron Dev.* **53** 2696
[21] Baczkowski L, Carisetti D, Jacquet J and Kendig D 2014 Thermal characterization of high power AlGaN/GaN HEMTs using infra red microscopy and thermoreflectance *20th Int. Workshop on Thermal Investigation of ICs and Systems (THERMINIC)* **vol 2014** pp 1–6
[22] Lee Y J, Lau B L, Leong Y C, Choo K F, Zhang X and Chan P K 2012 GaN-on-Si hotspot thermal management using direct die attached microchannel heat sink *Proc. 14th Electron. Packag. Technol. Conf. (EPTC)* pp 577–81
[23] Sarua A, Ji H, Kuball M, Uren M J, Martin T, Hilton K P and Balmer R S 2006 Integrated micro-Raman/infrared thermography probe formonitoring of self-heating in AlGaN/GaN transistor structures *IEEE Trans. Electron Devices* **53** 2438
[24] COMSOL Multiphysics reference manual, version 5.2, COMSOL AB, Stockholm, Sweden, www.comsol.com
[25] Nilsson O, Mehling H, Horn R, Fricke J, Hofmann R, Muller S G, Eckstein R and Hofmann D 1997 Determination of the thermal diffusivity and conductivity of monocrystalline silicon carbide (300–2300 K) *High Temp.–High Press.* **29** 73
[26] Cho J, Bozorg-Grayeli E, Altman D H, Asheghi M and Goodson K E 2012 Low thermal resistances at GaN–SiC interfaces for HEMT technology *IEEE Electron Dev. Lett.* **33** 378
[27] JMP® Version 8, SAS Institute Inc., SAS Campus Drive, Building T, Cary, NC 27513-2414, USA www.jmp.com
[28] Székely V 1997 A new evaluation method of thermal transient measurement results *Microelectron. J.* **28** 277